Nanotechnology **22** (2011) 115603 (9pp) doi:10.1088/0957-4484/22/11/115603

Synthesis of Ag–TiO_2 composite nano thin film for antimicrobial application

Binyu Yu[1], Kar Man Leung[2], Qiuquan Guo[1], Woon Ming Lau[3] and Jun Yang[1,2]

[1] Biomedical Engineering Graduate Program, The University of Western Ontario, London, ON, N6A 5B9, Canada
[2] Department of Mechanical and Materials Engineering, The University of Western Ontario, London, ON, N6A 5B9, Canada
[3] Surface Science Western, The University of Western Ontario, London, ON, N6A 5B9, Canada

Received 4 November 2010, in final form 28 December 2010
Published 4 February 2011
Online at stacks.iop.org/Nano/22/115603

Abstract

TiO_2 photocatalysts have been found to kill cancer cells, bacteria and viruses under mild UV illumination, which offers numerous potential applications. On the other hand, Ag has long been proved as a good antibacterial material as well. The advantage of Ag–TiO_2 nanocomposite is to expand the nanomaterial's antibacterial function to a broader range of working conditions. In this study neat TiO_2 and Ag–TiO_2 composite nanofilms were successfully prepared on silicon wafer via the sol–gel method by the spin-coating technique. The as-prepared composite Ag–TiO_2 and TiO_2 films with different silver content were characterized by scanning electron microscopy (SEM), atomic force microscopy (AFM), x-ray diffraction (XRD) and x-ray photoelectron spectroscopy (XPS) to determine the topologies, microstructures and chemical compositions, respectively. It was found that the silver nanoparticles were uniformly distributed and strongly attached to the mesoporous TiO_2 matrix. The morphology of the composite film could be controlled by simply tuning the molar ratio of the silver nitrate aqueous solution. XPS results confirmed that the Ag was in the Ag^0 state. The antimicrobial effect of the synthesized nanofilms was carried out against gram-negative bacteria (*Escherichia coli* ATCC 29425) by using an 8 W UV lamp with a constant relative intensity of 0.6 mW cm^{-2} and in the dark respectively. The synthesized Ag–TiO_2 thin films showed enhanced bactericidal activities compared to the neat TiO_2 nanofilm both in the dark and under UV illumination.

(Some figures in this article are in colour only in the electronic version)

1. Introduction

Researchers have shown constant interest in developing antimicrobial materials containing various organic chemical antibiotics and inorganic substances. Among these fine structural functional materials, nanosized organic and inorganic particles have attracted increasing attention in medical applications due to their unique properties and amenability to biological functionalization [1–3]. Compared with organic antimicrobial materials, the key advantages of inorganic antibacterial agents are improved safety and stability. Titanium dioxide (TiO_2) is one of the most effective photocatalysts currently in use due to its strong oxidizing power, non-toxicity and long-term physical and chemical stability. It has been widely used for the decomposition of organic compounds and microbial organisms, such as cancer cells, viruses and bacteria as well as its potential application in sterilization of medical devices and air-conditioning filters owing to its self-sterilizing property [4–7]. When irradiated with near UV light, TiO_2 exhibits strong bactericidal activity [8]. The photogenerated holes and electrons react with water and oxygen respectively to form hydroxyl radicals ($^{\cdot}OH$) and other reactive oxygen species, such as singlet oxygen (O_2^-), and hydrogen peroxide (H_2O_2) [9]. Thus, TiO_2 and TiO_2 deposited materials could kill bacteria and also simultaneously degrade the toxic compounds exhausted from the bacteria [7]. Complete oxidation of organic compounds and the whole cells to carbon dioxide can be achieved [10]. However, its drawbacks of the

low quantum yields and the lack of visible-light utilization hinder its practical application. To overcome these problems, numerous studies have recently been performed to enhance the photocatalytic efficiency and antibacterial activities, such as doping noble metals [11–14]. It is reported [15–17] that loading of silver nanoparticles highly enhances the photocatalytic activity of TiO_2. The enhancement is attributed to its ability to trap electrons at Schottky barriers at each Ag–TiO_2 contact region, which reduces the recombination of light generated e^-–h^+ at the TiO_2 surface. Therefore charge separation is promoted and more electron transfer occurs, and consequent longer electron–hole pair lifetimes.

Silver metal and silver solutions have been known as effective antimicrobial agents for centuries, owing to a broad spectrum of antibacterial activity as well as low toxicity towards cells [18]. Several studies have been reported to explain the inhibitory effect of silver on bacteria. In general, it is believed that silver ions interact with proteins by reacting with the SH groups present in bacteria, leading to the inactivation of the proteins [19]. Moreover, silver ions can interact with DNA of bacteria preventing cell reproduction [20]. Both effects lead to the death of the bacterial cells. In contrast to the use of silver ions, silver nanoparticles are long lasting, stable and are subject to controlled release. Especially with decreasing of the silver crystal size, there are more chemical reaction sites available. Silver-doped materials are chemically durable and release silver ions for a long time period. It is promising to fix silver nanoparticles on various supports [21–24], to perform as an excellent antibacterial coating in the food industry, water disinfection and other disinfection related fields.

The importance of silver in medical applications and the antibacterial activity of TiO_2 together led researchers to think about the manufacture of systems combining both titania and embedded silver compounds or silver nanoparticles, to expand the nanomaterial's antibacterial functions to a wider variety of working conditions. Synthesis of TiO_2/Ag nanocomposites has been carried out through different synthetic techniques. In the literature, a solvothermal method is commonly used to obtain the nanoparticles. But for practical applications, the sol–gel process is the most attractive method to introduce foreign metal ions into TiO_2 particles and films; for example, the photoreduction under UV exposure of Ag^+ containing films [25–28], and direct calcination of the sol–gel material [29–31]. However, photoreduced silver cannot be highly dispersed into the depth beneath the surface of TiO_2, especially when the adhesion force is weak for the coating surface. Moreover for the direct annealing methods, because of aggregation, agglomeration and other factors, the resultant composites showed a broad size distribution and non-uniform allocation of metal nanoparticles [25, 31]. Fortunately, these drawbacks could be suppressed by the use of the sonochemical method. Since the early 1980s, sol–gel processes in which precursor–water mixtures are exposed to intense ultrasonic irradiation have been investigated [32]. It has been demonstrated that the irradiated solution will result in higher density gel and less shrink during the following annealing process. Sonochemistry has been used not only for the preparation of the mesoporous materials, but also for the insertion of nanoparticles into the mesopores [33].

In this study, TiO_2 thin films deposited on silicon wafers with different silver content were prepared by a template sol–gel method. We could control the morphology of the composite films by tuning the molar ratio of water to Ti when introducing the silver ion. The interaction between the TiO_2 grains and the nanosized silver particles was enhanced by forming more hetero-junctions, such as Ag/anatase in the Ag–TiO_2 multiphase nanocomposite films. A low-intensity ultrasonic cleaning bath was used to help to highly disperse the silver ions. Different characterization methods were used to analyze the resultant films. The antibacterial effect of the obtained thin films on gram-negative bacteria was tested.

2. Materials and methods

2.1. Materials

Titanium (IV) isopropoxide (TTIP), $AgNO_3$, acetylacetone, poly(propylene glycol)-*block*-poly(ethylene glycol)-*block*-poly(propylene glycol) (P123, $M_n \sim 4400$) were all purchased from Sigma-Aldrich Chemical Co. The anhydrous ethanol was a commercial product and was used as received without further purification. Ultrapure Milli-*Q* water was used in all experiments. Gram-negative bacteria (*Escherichia coli* ATCC 29425) were used to test the antimicrobial activity of the resultant films. The strains were cultured in Nutrient Broth (BD Difco™) and Standard Methods Agar (BD Difco™) using the appropriate times and temperatures of incubation.

2.2. Preparation of silicon wafer supported TiO_2 and Ag–TiO_2 films

TiO_2 thin films were synthesized via a surfactant-templating method using a triblock copolymer (P123) as a template [34–36]. In a typical synthesis, 15 ml of titanium isopropoxide was added drop-wise to a template solution prepared by dissolving 10 g of P123 in 100 ml of absolute ethanol. Then 5 ml of acetylacetone was added to control the polymerization via the condensation rate. After stirring vigorously for 1 h at room temperature, 1 ml of water was added drop-wise to the solution under vigorous stirring. To form Ag nanoparticles embedded within the TiO_2 composite films, a solution B composed of an appropriate amount of $AgNO_3$ (the molar ratio of Ti to Ag was varied from 50:1 to 5:1) and 1 ml of deionized water was added drop-wise into the precursor solution under stirring. The mixture was sonicated at room temperature for 30 min using a low-intensity ultrasonic cleaner bath (Fisher FS 30 50/60 Hz 130 W). Then the resultant alkoxide solution was kept standing at room temperature for hydrolysis reaction for 1 h. The vigorous chemical reduction yields a brownish dispersion; there is a change of color (from yellow to brownish). All reactions containing $AgNO_3$ were conducted in amber glassware to prevent photoreduction of the silver ions. Samples with varying molar composition of Ti^{4+} to Ag^+ of 50:1, 20:1, 10:1 and 5:1, were named SG1, SG2, SG3 and SG4, respectively. The sample without the addition of silver nitrate was labeled as SG0.

The as-prepared sol could be applied onto different substrates by various techniques, such as dip-coating, a spraying process and spin coating. In our study, a spin processor (Laurell Technologies Corporation, PA) was used for the deposition of the solution onto washed silicon wafer. The silicon wafer substrates were cleaned in a piranha solution (7:3 concentrated H_2SO_4/H_2O_2) for 1 h at 90 °C, followed by thorough rinsing with distilled water and dried under a stream of nitrogen. 100 μl of precursor solution, prepared according to the procedure described above, was applied onto modified silicon wafer (160 × 160 mm^2) by spin-coating at 2500 rpm for 30 s. The obtained films were typically dried at 100 °C for 30 min and then heat-treated at 500 °C for 1 h (1 °C min^{-1}) and cooled to ambient temperature. The thickness of the resultant films was controlled by repeating the cycle three times from spinning to heat treatment. Silver only samples were also prepared through the same process without adding TTIP.

2.3. Materials characterization

The crystalline structures of the Ag–TiO_2 and TiO_2 films were determined by x-ray diffraction (XRD) with Co (λ = 1.790 26 Å) radiation operated at 45 kV and 160 mA with a rotating anode x-ray generator (Rigaku Rotaflex RTP 30). The scanning range was from 20° to 75°. The surface compositions were characterized by x-ray photoelectron spectroscopy (XPS; Kratos Axis Ultra spectrometer, Surface Science) using Al Kα (E = 1486.6 eV). All the binding energies were referenced to the C 1s peak at 284.8 eV of the surface adventitious carbon. The as-deposited surface was etched by Ar ion sputtering at an energy of 4 keV for 5 min to analyze the chemical state of the Ag–TiO_2 films. Survey scan analyses were carried out with an analysis area of 300 μm × 700 μm. The surface morphology of the films was assessed by scanning electron microscopy (SEM; HITACHI S-4500) with an energy-dispersive x-ray spectrometer (EDX). The cross-section of the samples was covered by a Pt layer to increase the conductivity. The surfaces were further visualized by an atomic force microscope (AFM). Images were obtained by scanning a surface of 1 μm × 1 μm in a tapping mode using silicon nitric cantilevers with a spring constant of 40 N m^{-1} at ambient conditions.

2.4. Measurements of photoinduced super-hydrophilicity

The surface wettability was measured in ambient air at room temperature using a contact angle meter (Model 100-00 contact angle goniometer) based on the sessile drop method. The photoinduced hydrophilicity of the resultant films was also evaluated by the water contact angle difference before and after illumination with an 8 W UV lamp (emission in 340–400 nm, with a peak at 365 nm, UVP, Inc. Upland, CA, USA). The droplet size used for the measurements was 8 μl. At least five measurements on each sample were recorded and the average value was adopted as the static contact angle.

2.5. Antibacterial activity evaluation

The bacteria were cultivated in Nutrient Broth medium at 37 °C for 18–24 h, and then harvested by centrifugation at 3000 rpm for 10 min. After removing the supernatant, the cells were washed with phosphate buffer solution (PBS) twice and were resuspended with the same PBS solution. The final concentration of bacterial cells was diluted to approximately 2×10^6–2×10^5 CFU ml^{-1} with PBS solution. The antibacterial activity of the coatings against *E. coli* was determined by two different methods: (i) qualitative evaluation using the zone of inhibition method and (ii) quantitative evaluation.

For the qualitative evaluation (zone of inhibition test), 20 ml of liquid nutrient agar was poured onto disposable sterilized Petri dishes and allowed to solidify. Then 100 μl of the bacterial PBS solution (10^6 CFU ml^{-1}) was streaked over the plate and spread uniformly. Both the silicon wafer substrates coated with Ag–TiO_2 and pure TiO_2 films were gently placed over the solidified agar gel in different Petri dishes. The plates were incubated at 37 °C for 24 h and the antagonistic activity was estimated by a clear zone of inhibition around the coated substrate. Uncoated silicon wafers were also tested as negative controls.

In order to quantitatively evaluate the antibacterial activity, samples were investigated both under low-intensity UV light and in the dark. For the antibacterial evaluation under the UV light, an 8 W UV lamp (emission in 340–400 nm, with a peak at 365 nm, UVP, Inc. Upland, CA, USA) was used as the light source. The sample was placed in a sterilized Petri dish. Then 100 μl of PBS solution containing bacteria was added drop-wise onto the surface of each sample. The Petri dish was sealed and illuminated with UV light from above. The light intensity at the working films was 0.6 mW cm^{-2} measured by a UV intensity meter (Model 1000 SUSS Micro Tec, Inc.). To measure the antibacterial activity in the dark, the experiment was carried out under similar conditions without illumination. After a certain period the bacteria containing drops were washed from the surface of the sample by using 10 ml PBS in the sterilized Petri dish. Then 100 μl of each bacteria suspension was dispersed on the plate count agar. The number of surviving bacterial colonies on the Petri dish was counted after incubation for 24 h at 37 °C. The counts on three plates corresponding to a particular sample were averaged.

3. Results and discussion

3.1. Characterization of the TiO_2 and Ag–TiO_2 films

3.1.1. XRD and XPS analysis. The x-ray diffraction patterns of the resultant films (figure 1) showed that six typical TiO_2 peaks can be attributed to the (101), (004), (200), (105), (211) and (204) crystal planes, respectively. This indicated that all the resultant films exhibit a pure anatase phase structure. For all the composite films after heat treatment at 500 °C for 1 h, no crystalline phase of metallic silver formation was detected. This may due to the uniform distribution of silver nanoparticles in the titanium matrix, or the peak of silver at 2θ = 44.3° was covered by the peak of TiO_2 at 2θ = 44.47° owning to the low content of silver. Similar behavior was also reported by Chang *et al* [37]. Different from the previous study [31], the presence of silver content does not lead to apparent varieties in crystalline structure. There is no significant reduction in particle size observed with the increase of silver amount.

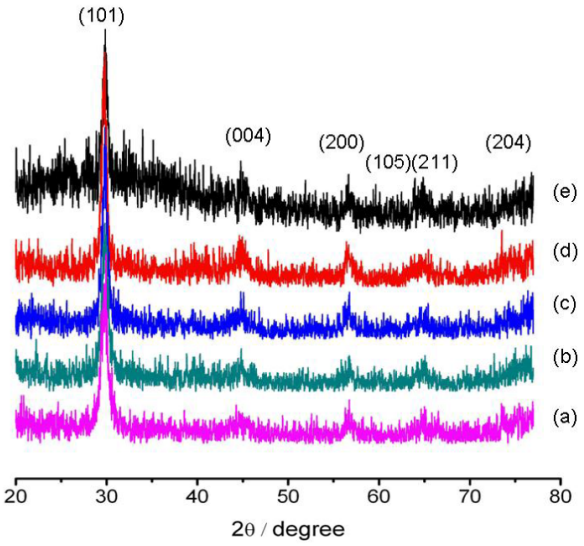

Figure 1. Wide-angle x-ray scattering patterns of the result films with different Ag contents: samples SG0–SG4 are labeled as (a)–(e) in sequence.

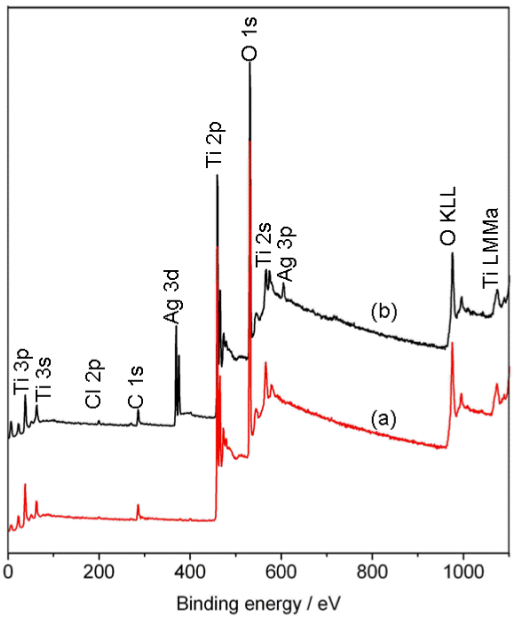

Figure 2. XPS spectra of TiO_2 (a) and Ag–TiO_2 (b) composite films of SG4.

To confirm the metallic state of the silver on the surface of these samples, the resultant film samples were further characterized by XPS measurement. Figure 2 shows the XPS profiles of the prepared TiO_2 and Ag–TiO_2 composite films. The peak position of 368.5 eV for Ag^0 was taken as the reference value. The Ag element clearly appeared on the surface of the Ag–TiO_2 composite thin films. The XPS spectra of Ag $3d_{5/2}$ of the fresh SG4 sample right after the calcination process were recorded. As shown in figure 3, XPS spectra of the fresh SG4 samples before and after 8 W UV lamp exposure were fitted with a nonlinear least-squares fitting program. The Ag $3d_{5/2}$ peak appeared at a binding energy of 368.5 eV. This binding energy indicated that the silver was of metallic nature [38]. After 0.6 mW cm^{-2} UV exposure for 1 h, the XPS spectra of Ag $3d_{5/2}$ indicated that there were two components after deconvolution, ascribed to Ag_2O (367.9 eV) and Ag^0 (368.6 eV) respectively [38]. The Ag species mainly exist as Ag_2O after UV exposure, while there is still Ag^0 on the surface. Thus we may conclude that metallic silver is oxidized due to the strong oxidation ability of the TiO_2 matrix under UV exposure.

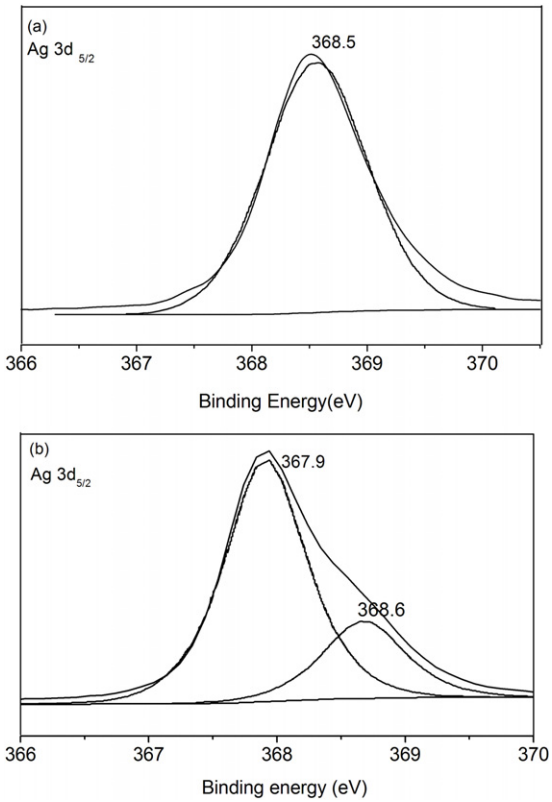

Figure 3. High-resolution XPS spectra of Ag $3d_{5/2}$ in the Ag–TiO_2 composite film SG4. (a) Before UV exposure and (b) after 0.6 mW cm^{-2} UV exposure for 1 h.

3.2. SEM/EDX analysis

SEM images of the pure TiO_2 and the composite films with different silver content are presented in figure 4. While all the films were sintered at 500 °C, the morphology of the constituted grains seems to be different dependent on the Ag content. The image of the pure TiO_2 film (figure 4(a)) illustrates an extremely smooth and dense surface. There are no defects observed, and the average size of the TiO_2 granular structure is approximately 20 nm in diameter. Considering that heavy elements (e.g. Ag) backscatter electrons more strongly than light elements (e.g. O, Ti), the metallic silver appears brighter in the image. At low $AgNO_3$ concentrations, the shining Ag nanoparticles with a diameter around 20–30 nm were well dispersed as shown in figures 4(b) and (c). The surface of SG1 is very similar to that of SG2; and the density of Ag nanoparticles was increased with respect to SG2 due to the Ag^+ concentration being increased in the sol

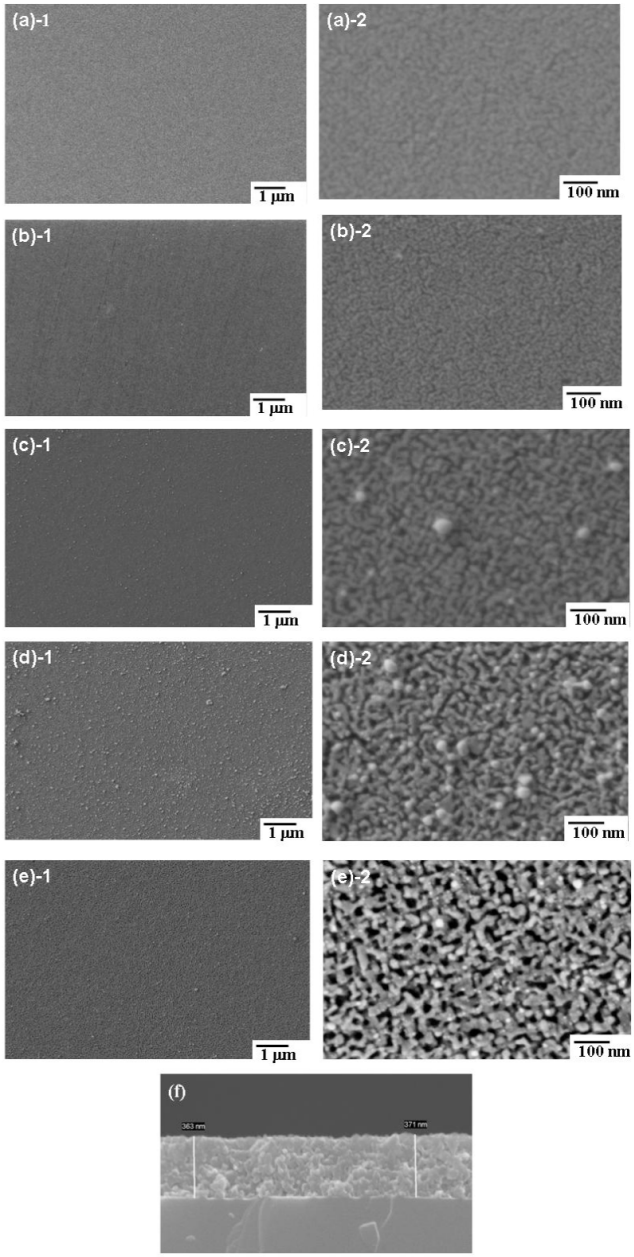

Figure 4. Scanning electron micrographs of (a) the neat TiO_2 film surface of SG0, (b) SG1, (c) SG2, (d) SG3 and (e) SG4 Ag–TiO_2 composite film surfaces. (a)-2, (b)-2, (c)-2, (d)-2 and (e)-2 are enlarged images of (a), (b), (c), (d) and (e) respectively. (f) The thickness of the films is about 370 nm as determined by the cross-section image.

solution. The TiO_2 substrate films are still smooth and worm-like TiO_2 grains appear. For a higher silver concentration, the Ag nanoparticles became gradually aggregated but still remained roughly uniform on the surface as shown in figure 4(d)-1. Instead of having a smooth surface, the Ag–TiO_2 composite films displayed a rough surface morphology. The addition of silver salt results in a more mesoporous TiO_2 matrix (figure 4(d)-2), which includes TiO_2 crystallites of 10–20 nm in size and small Ag nanoparticles (white spots) with various sizes ranging from 10 to 30 nm. Finally, when the concentration increased further, no obvious aggregation was observed on the surface (figure 4(e)-1). The enlarged image (figure 4(e)-2) shows the smaller Ag nanoparticles more uniformly distributed in the TiO_2 matrix. Although the size of the silver particles is smaller with diameter around 10 nm, there are more nano-pores detected in the thin film. It is reported that heating promotes aggregation of Ag atoms. As the radius of Ag^+ ions (ca. 126 pm) is much larger than that of Ti^{4+} (ca. 68 pm), the Ag^+ ions introduced by the sol–gel process would not enter into the lattice of the TiO_2 anatase phase [39]. When the samples were heat-treated to a certain temperature, the reduction of Ag^+ to Ag^0 took place as the $AgNO_3$ decomposed. During the calcination process, these uniformly dispersed Ag^+ ions would gradually migrate along with the anatase grain boundaries to the surface of the TiO_2 film, while TiO_2 anatase grains would grow at the same time. Finally, the Ag^+ ions probably exist on the surface of the anatase grains by forming Ag–O–Ti bonds. In our present study, the movement of the resulting nanoparticles in the TiO_2 matrix could also be restricted by tuning the molar ratio of water to Ti when adding the Ag^+ preparing sol, and hence particle aggregation is controlled. The anatase grain growth is thereby depressed and the specific surface area increases. The porous feature of the film indicates that it should have a rough surface.

Spin-coating resulted in TiO_2 and Ag–TiO_2 thin films with a thickness of approximately 370 nm as determined from the cross-section images (figure 4(f)). From spin-coating theory, the resultant film thickness is mainly decided by two factors: liquid viscosity and rotating speed. In our case, the rotating speed was kept the same and the viscosity of the precursor solution did not change much as the silver concentration changed. Hence the film thickness could be kept the same.

EDX spectra of the film show the presence of a small amount of silver within the surface. Quantification of the spectra indicates that the silver content varies with the different $AgNO_3$ amount and the molar ratios of Ti to Ag are around 4.5:1 and 13:1 in SG4 and SG3 respectively as shown in table 1. This is in good agreement with theoretically calculated values of the precursor solution composite.

Table 1. Composition of Ag–TiO_2 composite films according to EDX analysis.

Sample	O	Si	Ti	Ag
SG0	31.48	58.98	9.54	—
SG3	34.94	53.06	11.16	0.85
SG4	31.01	56.49	10.21	2.28

3.3. AFM

AFM was used to characterize the morphology and surface roughness of the samples. Figure 5 shows the representative top view images and angle view images of the surface morphology of a scan area 1 μm × 1 μm of the Ag–TiO_2 composite films on silicon wafers by three spin-coating cycles. It is clear to see from the height images that the surface of SG2 is smooth with an rms roughness of 1.22 nm. The AFM image

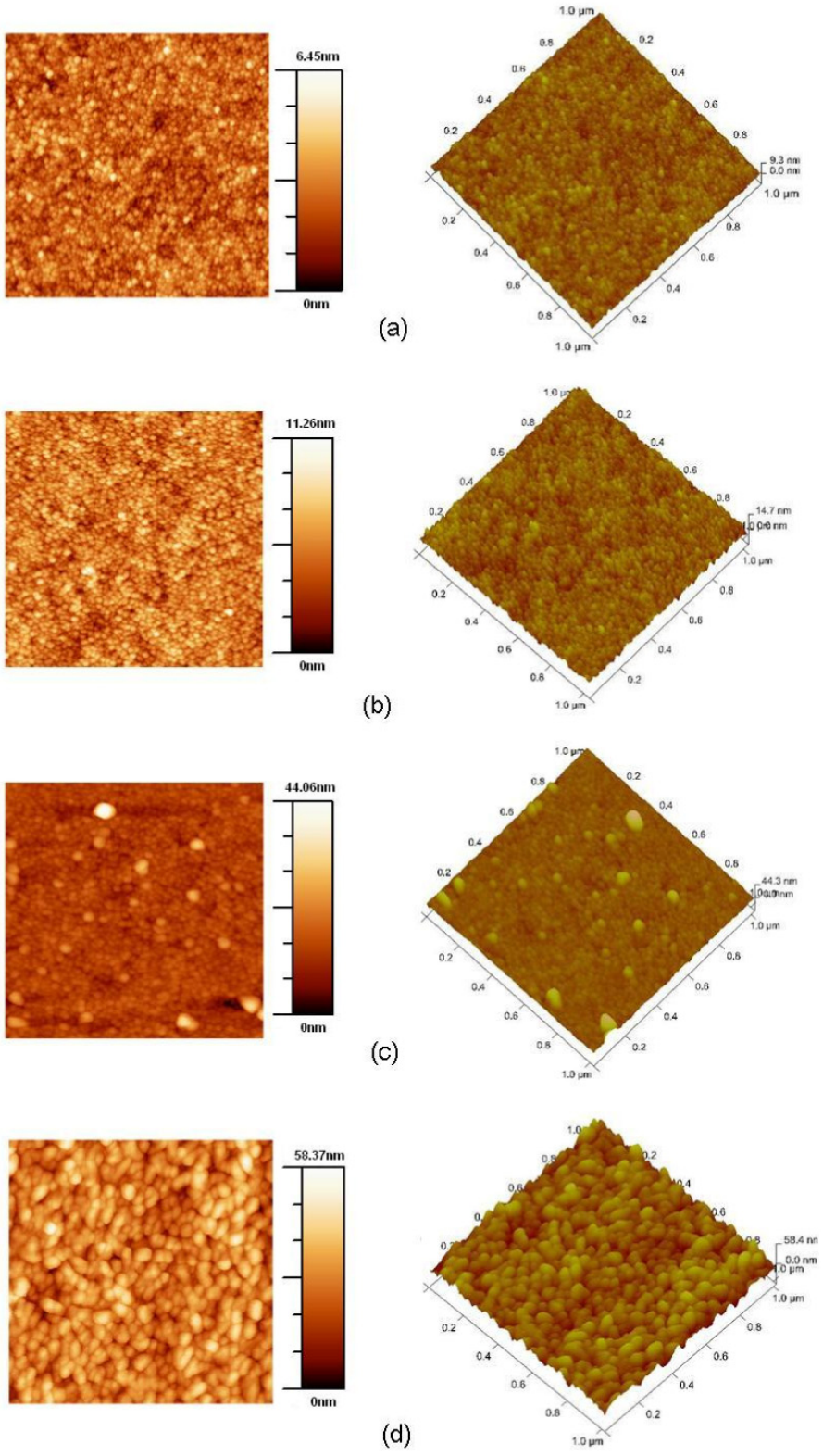

Figure 5. AFM top view images (left) and AFM angle view images (right) of the composite films SG0 (a), SG2 (b), SG3 (c) and SG4 (d).

confirms the results obtained by SEM since the surface of SG3 is covered with some silver particles with diameter of around 30 nm. The statistical mean roughness of the surface is about 3.44 nm, while the maximum height within this area is about 30 nm. As for the sample SG4 with the highest silver content, no obvious silver aggregation was observed, indicating that silver nanoparticles uniformly dispersed in the matrix without aggregation. This result is in general agreement with the SEM observation. The height image of SG4 shows a mesoporous surface structure with an rms about 8.57 nm. The grain size of

Table 2. Surface roughness of the resultant films with different silver contents.

Sample	R_q^a	R_a^b
SG0	0.859	0.677
SG2	1.222	0.965
SG3	3.440	2.020
SG4	8.570	6.710

[a] Mean square roughness of resultant films.
[b] Average roughness of resultant films.

TiO_2 estimated from AFM images was quite large, which may be due to the worm-like structure as shown in the SEM image and the silver nanoparticles embedded within the TiO_2 matrix. The average roughness (R_a) and mean square roughness (R_q) of the resultant films are listed in table 2.

3.4. Hydrophilicity

The photoinduced hydrophilicity of TiO_2 via UV light irradiation is well known. It is assumed that photogenerated holes lead to the oxidation of the bridging oxygen (O_2^-) to oxygen and generate oxygen vacancies simultaneously. The adsorption of water molecules on the surface was dissociated via the oxygen vacancies under UV illumination. This process created hydrophilic OH groups on the illuminated TiO_2 surface [40]. Prior to UV light irradiation, the freshly prepared neat TiO_2 film showed a highly hydrophilic property, with the water contact angle around 15° ± 2°. It was observed that the water contact angles of the composite films were 20° ± 2° for SG1 and SG2, 25° ± 2° for SG3 and SG4 respectively. However, the water contact angle of all the resultant films could drop to 5° ± 2° after 2 h UV irradiation of 0.6 mW cm^{-2} in ambient conditions. It is known that the wettability of a solid surface is influenced by both surface energy and the geometrical microstructure of the surface. It is expected that the initial water contact angle varies with the composite films of different surface roughness. The loading of silver has no effect on the photoinduced hydrophilicity of TiO_2. Moreover, the composite films of higher silver loading showed higher hydrophilicizing rate. The water contact angle tended to increase up to a certain angle due to gradual adsorption of contaminants on the surface, which make the surface more hydrophobic. However, the water contact angle could be recovered by UV illumination again. In our case, the water contact angle would drop from 40°–25° to 8°.

3.5. Antibacterial activity evaluation

The antibacterial activity is evidenced by an inhibition zone of bacteria (*E. coli*) growth around the resultant substrates as shown in figure 6 as a typical result. No bacterial growth was observed on the top of and adjacent to the Ag–TiO_2 coatings. The result demonstrates that all the composite films could inhibit the bacterial growth. Bacterial growth was seen around and on the top of the neat TiO_2 coated substrate without UV exposure, as indicated by the presence of colonies. Table 3 presents the experimental results for the qualitative evaluation. The diameter of the inhibition zone increases from 0.3 to 0.7 cm with the growing silver loaded in the composite films. This result was expected, because the driving force of silver ion diffusion from the bulk to the surface is larger for films with higher silver content. Ag only samples without the TiO_2 matrix with the same silver content in solution as their counterparts of the composite films SG2 and SG4 did not show clear inhibition zones. For the present method of material synthesis, the silver only samples appeared as bulk silver or

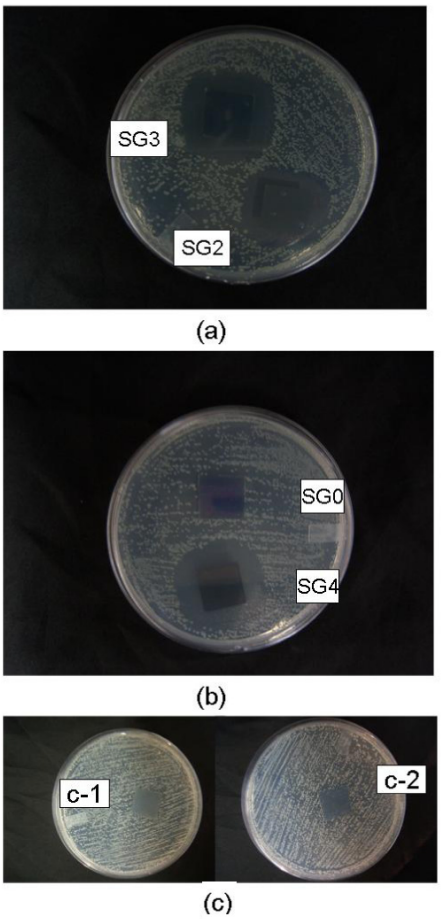

Figure 6. Zone of inhibition test results. Comparison of the composite Ag–TiO_2 film and the neat TiO_2 film for *E. coli* with agar plating. C-1 and C-2 are silver only samples without the TiO_2 matrix for the same silver content in solution as their counterparts of the composite films SG4 and SG2 respectively.

Table 3. The antibacterial test result of the composite films with different silver contents against *E. coli*.

Sample	Diameter of inhibition zone (cm)[a,b]
SG0	0
SG1	0.25(0.05)
SG2	0.50(0.05)
SG3	0.65(0.05)
SG4	0.7(0.06)

[a] Duplicate experiments gave similar results.
[b] Standard deviations are given in parentheses.

silver crystal aggregations, which lead to very limited silver ion diffusion. While in the Ag–TiO_2 composite films the silver appeared as 10–30 nm nanoparticles and was well dispersed in the TiO_2 matrix, the Ag–TiO_2 composite films exhibited much larger inhibition zones. These results indicate that the diffusion of silver ions may depend on the formation of silver in the nanofilms. In this work, silver ion diffusion has been evaluated in the sample SG4 by ICP-AES (inductively coupled plasma atomic emission spectroscopy). To avoid the possible formation of insoluble salt crystals on the coating surface in the saline solution, we chose deionized water as test fluid to evaluate the silver ion release. Non-cumulative release of silver ions into 50 ml of deionized water from 10 cm^2 and 370 nm thick SG4 Ag–TiO_2 composite film was recorded, whose concentration was 0.4 ppm, 0.26 ppm and 0.005 ppm for 1 h, 24 h and 7 days after immersion, respectively.

As expected, the composite film with the highest silver loading (SG4) showed the most notable antibacterial effect and the inhibition zone diameter increased about three times compared to SG1. The actual antibacterial mechanism of silver nanoparticles is still under debate. Some research results have suggested the silver might be used as a metal, but the active agent appears to be the ions produced. In the presence of water and oxygen, silver particles release small amounts of silver ions [41], which induce the cell death. While a study by Panacek [42] suggested that the silver nanoparticles might attach on the surface of the cell membrane, affecting the permeability and respiration. The interactions of the silver nanoparticles with the bacteria are dependent on the size and shape of the nanoparticles. In our experiment, the observed inhibition zone is a result of the leaching of active biocidal Ag^+ ions from the embedded silver nanoparticles present in the composite coating matrix into the surrounding aqueous medium, which cause the bacteria death.

On the basis of the qualitative results, quantitative tests were carried out on the films of SG0, SG2, SG3 and SG4. Figure 7 shows the bacteria killing ratio under UV light illumination and in the dark. After 1 h UV exposure the viable count for *E. coli* showed almost 100% bacterial killing by the sample SG4, while under the same conditions the neat TiO_2 (SG0) film showed a decrease of about 60% only. The samples SG2 and SG3 with less silver content showed decreases of 78% and 90%, respectively. The bactericidal effect of TiO_2 under UV irradiation has been well documented [7]; the UVA light intensity, the extent of irradiation and the catalyst concentration play important roles in the disinfection properties. It is reported that anatase TiO_2 film exhibits a strong photocatalytic reaction under UVA illumination and the bactericidal activity of TiO_2 is directly related to ultraviolet light absorption and the formation of various reactive species such as superoxide radicals and hydroxyl radicals [11], so in the dark TiO_2 particles present no bactericidal activity. Furthermore, silver ions are also photoactive in the presence of UVA and the photochemical reaction of the silver–cysteine complex hinders the enzymatic function of the affected protein, leading to enhanced inactivation of bacteria [43]. The silver only film prepared from the highest silver nitrate concentration showed 63 ± 15% decrease after 1 h UV of illumination and 39 ± 16% decrease in the dark respectively. The Ag–TiO_2 composite film SG4 with the richest content of silver nanoparticles also showed the highest antimicrobial activity against *E. coli* in the dark and at least 80% decrease in terms of the number of grown bacterial colonies was found, while SG2 and SG3 showed decreases of 45%, and 63.5% respectively after a 1 h interaction. For the neat TiO_2 coating, the decrese of the number of viable cells by 5% is caused by natural apoptosis. In our study, 0.6 mW cm^{-2} UV light intensity was chosen and the blank washed silicon under the same UV illumination was considered as the blank control. The control result showed around 13% inactivation of *E. coli* after 1 h of UV irradiation. This could be explained by the exposure to long wavelength UV light, which damaged organisms by exciting photosensitive molecules within the cell to produce active species to damage the genome and other intracellular molecules [44].

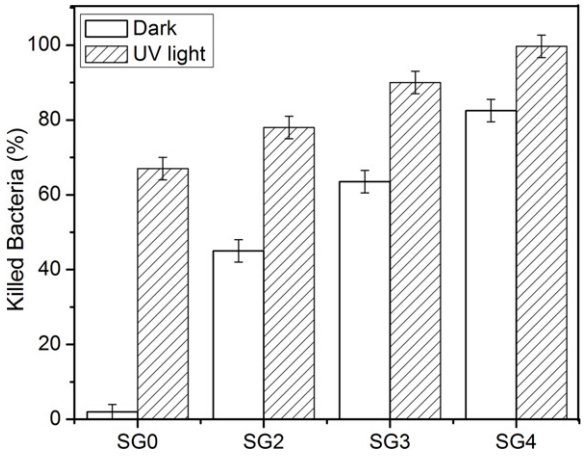

Figure 7. Killing ratio of *E. coli* in the liquid film on Ag–TiO_2 composite film and neat TiO_2 film under 1 h of UV light illumination (0.6 mW cm^{-2}) and in the dark for 1 h. For the blank silicon wafer, the killing ratio is 13 ± 5% under the same UV irradiation.

The above results exhibited that all the Ag–TiO_2 composites have antibacterial activity even when no light is present, indicating that the silver nanoparticles were responsible for the antimicrobial effect of the coatings in the dark. The higher antibacterial activity of the composite films under the UV light is due to the synergistic antibacterial effects of the photocatalytic reaction of the TiO_2 coating and silver nanoparticles in the matrix. After storing for two months in the dark in an atmospheric environment, the Ag–TiO_2 composite film SG2 showed 76.7 ± 3% and SG4 showed 99.7 ± 2% inactivation of *E. coli* after 1 h of UV exposure. This indicated the stability of the Ag–TiO_2 composite film. The advantage of Ag–TiO_2 nanocomposite is to expand the antibacterial nanomaterial's functions to a wider variety of working conditions. Thus, the present Ag–TiO_2 composite films are effective in diminishing the living cells and are promising as antibacterial coatings. More detailed silver ion release tests combined with antimicrobial dynamic tests and anti-biofilm properties of the resultant films will be studied in further work.

4. Conclusion

Mesoporous TiO_2 thin films of polycrystalline anatase containing silver nanoparticles were prepared by the template sol–gel method on silicon substrates. The morphology of the obtained films could be tuned by changing the ratio of water to Ti in the precursor solution. Silver nanoparticles can be uniformly distributed and strongly attached to the mesoporous TiO_2 matrix. The inactivation of *E. coli* in the dark and under UVA illumination of the composite films with different silver loadings was compared. The composite films display excellent antibacterial activity and better antibacterial effect with increase of the silver content of the samples. A similarly strong antimicrobial property was observed even after the composite films were stored for long periods. The synthesis process is simple, convenient and low cost. It may be reasonably presumed that such mesoporous TiO_2 substrates with silver loaded composite films will prolong the release time of silver ions and preserve the sustained antibacterial behavior. However, further studies must be conducted to examine silver ion release kinetics combined with an antimicrobial efficacy test and the cytotoxicity of the composite films. Such mesoporous TiO_2 substrate structures with silver loading could have promising applications as antibacterial materials for biomedical use and in the water treatment field.

Acknowledgments

J Yang is grateful for the financial support from The Interdisciplinary Development Initiatives (IDI) Program, Natural Science and Engineering Research Council of Canada (NSERC) and Canada Foundation for Innovation (CFI) for equipment. B Yu is grateful for the support from the Ontario Graduate Scholarship Program.

References

[1] Shi Z L, Neoh K G, Kang E T and Wang W 2006 *Biomaterials* **27** 2440–9
[2] Cioffi N, Torsi L, Ditaranto N, Tantillo G, Ghibelli L, Sabbatini L, Bleve-Zacheo T, D'Alessio M, Zambonin P G and Traversa E 2005 *Chem. Mater.* **17** 5255–62
[3] Vigneshwaran N, Kumar S, Kathe A A, Varadarajan P V and Prasad V 2006 *Nanotechnology* **17** 5087–95
[4] Sunada K, Watanabe T and Hashimoto K J 2003 *J. Photochem. Photobiol.* A **156** 227–33
[5] Blake D M, Maness P C, Huang Z, Wolfrum E J and Huang J 1999 *Sep. Purif. Methods* **28** 1–50
[6] Nonami T, Hase H and Funakoshi K 2004 *Catal. Today* **96** 113–8
[7] Sunda K, Kikuchi Y, Hashimoto K and Fujishima A 1998 *Environ. Sci. Technol.* **32** 726–8
[8] Fujishima A, Rao T N and Tryk D A 2000 *J. Photochem. Photobiol.* C **1** 1–21
[9] Mills A and Hunte S Le 1997 *J. Photochem. Photobiol.* A **108** 1–35
[10] Jacoby W A, Maness P C, Wolfrum E J, Blanke D M and Fennel J A 1998 *Environ. Sci. Technol.* **32** 2650–3
[11] Fu G F, Vary P S and Lin C T 2005 *J. Phys. Chem.* B **109** 8889–98
[12] Choi W, Termin A and Hoffmann M R 1994 *J. Phys. Chem.* **98** 13669–79
[13] Cozzoli P D, Comparelli R, Fanizza E, Curri M L, Agostiano A and Laub D 2004 *J. Am. Chem. Soc.* **126** 3868–79
[14] Mayya K S, Gittins D I and Garuso F 2001 *Chem. Mater.* **13** 3833–6
[15] Zhao G, Kozuka H and Yoko T 1996 *Thin Solid Films* **277** 147–54
[16] Coleman H M, Chiang K and Amal R 2005 *Chem. Eng. J.* **113** 65–73
[17] Tada H, Teranishi K, Inubushi Y I and Ito S 2000 *Langmuir* **16** 3304–9
[18] Berger T J, Spadaro J A, Chapin S E and Becker R O 1976 *Antimicrob. Agents Chemother.* **9** 357–8
[19] Lehninger A L, Nelson D L and Cox M M 1993 *Principles of Biochemistry* 2nd edn (New York: Worth)
[20] Feng Q L, Wu J, Chen G Q, Cui F Z, Kim T N and Kim J O 2000 *J. Biomed. Mater. Res.* A **52** 662–8
[21] Dai J and Bruening M L 2002 *Nano Lett.* **2** 497–501
[22] Hyung J J, Sung C Y and Seong G O 2003 *Biomaterials* **24** 4921–8
[23] Yuranova T, Rincon A G, Pulgarin C, Laub D, Xantopoulos N, Mathieu H J and Kiwi J 2006 *J. Photochem. Photobiol.* A **181** 363–9
[24] Lv Y H, Liu H, Wang Z, Liu S J, Hao L J, Sang Y H, Liu D, Wang J Y and Boughton R I 2009 *J. Membr. Sci.* **331** 50–6
[25] Hermann J M, Tahiri H, Ait-Ichou Y, Lassaletta G, González-Elipe A R and Fernández A 1997 *Appl. Catal.* B **13** 219–28
[26] Naoi K, Ohko Y and Tatsuma T 2005 *Chem. Commum.* **10** 1288–90
[27] Kubo W and Tatsuma T 2005 *J. Mater. Chem.* **15** 3104–8
[28] Xin B F, Jing L Q, Ren Z Y, Wang B Q and Fu H G 2005 *J. Phys. Chem.* B **109** 2805–9
[29] He C, Yu Y, Hu X F and Larbot A 2002 *Appl. Surf. Sci.* **200** 239–47
[30] Sen S, Mahanty S, Roy S, Heintz O, Bourgeois S and Chaumont D 2005 *Thin Solid Films* **474** 245–9
[31] Seery M K, George R, Floris P and Pillai S C 2007 *J. Photochem. Photobiol.* A **189** 258–63
[32] De la Rosa-Fox N, Esquivias E and Pinero M 2001 *Handbook of Organic–Inorganic Hybrid Materials and Nanocomposites* vol 1, ed H S Nalwa (Los Angeles: Academic, Stanford Scientific Corp.)
[33] Yu J C, Wang X C, Wu L, Ho W K, Zhang L Z and Zhou G T 2004 *Adv. Funct. Mater.* **14** 1178–83
[34] Yang P D, Deng T, Zhao D Y, Feng P Y, Pine D, Chmelka B F, Whitesides G M and Stucky G D 1998 *Science* **282** 2244–6
[35] Frindell K L, Bartl M H, Popitsch A and Stucky G D 2004 *Angew. Chem. Int. Edn* **41** 959–62
[36] Yu J C, Wang X C and Fu X Z 2004 *Chem. Mater.* **16** 1523–30
[37] Chang C C, Chen J Y, Hsu T L, Lin C K and Chan C C 2008 *Thin Solid Films* **516** 1743–47
[38] Moulder J F, Stickle W F, Sobol P E and Bomben K D 1992 *Handbook of X-ray Photoelectron Spectroscopy* (Eden Prairie, MN: Perkin-Elmer)
[39] Kingery W D, Bowen H K and Uhlmann D R 1976 *Introduction to Ceramics* (New York: Wiley)
[40] Sakai N, Fujishima A, Watanabe T and Hashimoto K 2001 *J. Phys. Chem.* B **105** 3023–6
[41] Hu C, Lan Y Q, Qu J H, Hu X X and Wang A M 2006 *J. Phys. Chem.* B **110** 4066–72
[42] Panacek A, Kvitek L, Prucek R, Kolar M, Vecerova R, Pizurova N, Sharma V K, Nevecna T and Zboril R 2006 *J. Phys. Chem.* B **110** 16248–53
[43] Kim J Y, Lee C, Cho M and Yoon J 2008 *Water Resour.* **42** 356–62
[44] Oguma K, Katayama H and Ohgaki S 2002 *Appl. Environ. Microbiol.* **68** 6092–35